

# Controlled Generation of Chimera States in SQUID Metasurfaces using DC Flux Gradients

N. Lazarides<sup>1,2</sup>, J. Hizanidis<sup>1,2</sup>, G. P. Tsironis<sup>1,2</sup>

<sup>1</sup>*Department of Physics, University of Crete, P. O. Box 2208, 71003 Heraklion, Greece;*

<sup>2</sup>*National University of Science and Technology "MISIS", Leninsky Prospekt 4, Moscow, 119049, Russia*  
(Dated: February 6, 2019)

SQUID (Superconducting QUantum Interference Device) metamaterials, subject to a time-independent (dc) flux gradient and driven by a sinusoidal (ac) flux field, support chimera states that can be generated with zero initial conditions. The dc flux gradient and the amplitude of the ac flux can control the number of desynchronized clusters of such a generated chimera state (i.e., its “heads”) as well as their location and size. The combination of three measures, i.e., the synchronization parameter averaged over the period of the driving flux, the incoherence index, and the chimera index, is used to predict the generation of a chimera state and its multiplicity on the parameter plane of the dc flux gradient and the ac flux amplitude. Moreover, the full-width half-maximum of the distribution of the values of the synchronization parameter averaged over the period of the ac driving flux, allows to distinguish chimera states from non-chimera, partially synchronized states.

PACS numbers: 05.45.Xt, 41.20.-q, 78.67.Pt, 85.25.Dg, 89.75.-k

Keywords: Superconducting metamaterials, SQUID metasurfaces, Chimera states, Flux gradient

## I. INTRODUCTION.

SQUID (Superconducting QUantum Interference Device) metamaterials have been investigated intensively both experimentally and theoretically the last decade [1–3], revealing a number of extraordinary properties. From the dynamical systems point of view, SQUID metamaterials are extended systems of identically coupled, highly nonlinear oscillators. Interestingly, they support counter-intuitive spatiotemporal states such as *chimera states*, as it was demonstrated numerically both for locally and nonlocally coupled SQUIDs in one and two dimensions [4–7]. Chimera states have attracted great attention by the scientific community since their discovery [8] from both theoretical and experimental viewpoints [9–11]. In the present case they are characterized by the coexistence of clusters of SQUIDs, in which flux oscillations are synchronized and desynchronized.

There have been several attempts to control the emergence and stability of chimera states through, e.g., the introduction of excitable units in FitzHugh-Nagumo networks [12], by feedback in coupled phase oscillators [13, 14], by using spatial pinning in a ring of nonlocally coupled oscillators [15], or by using gradient dynamics in non-locally coupled rings [16]. Here, the generation and control of chimera states in two-dimensional (2D) SQUID metamaterials (SQUID metasurfaces) driven by a sinusoidal (ac) flux field and biased by a time-independent (dc) flux gradient is demonstrated numerically. Moreover, they are generated without the need for a specific choice of initial conditions. Note that the application of a dc flux gradient to a SQUID metamaterial is experimentally feasible with existing experimental set-ups [17]. The size, location, and the number of desynchronized clusters (i.e., the multiplicity) of the generated chimera states can be controlled by the dc flux gradient and the ac flux amplitude. Such spatially inhomogeneous states can be in

principle detected and visualized using a recently developed method that relies on the cryogenic Laser Scanning Microscope (LSM) [18–20].

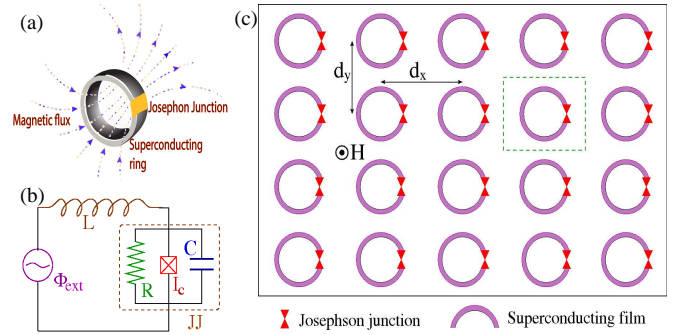


FIG. 1: (Color online) (a) Schematic of a superconducting quantum interference device (SQUID) in a magnetic field. (b) Equivalent electrical circuit. (c) Schematic of a two-dimensional SQUID metamaterial (SQUID metasurface).

## II. FLUX DYNAMICS EQUATIONS.

A simple version of a SQUID, consisting of a superconducting ring interrupted by a Josephson junction (JJ) [21], is shown schematically in Fig. 1(a). Its equivalent electrical circuit model features a self-inductance  $L$ , a capacitance  $C$ , a resistance  $R$ , and a critical current  $I_c$ , which characterizes the JJ (Fig. 1(b)). SQUIDs have been studied for many years and they have found numerous applications in magnetic field sensors, biomagnetism, non-destructive evaluation, and gradiometers, among others [22, 23]. They exhibit rich dynamic behavior including multistability, complex bifurcation structure, and chaos [24]. The multistability property, in particular, favors the emergence of chimera states in SQUID

metamaterials/metasurfaces [5, 6].

Consider a planar SQUID metamaterial (Fig. 1(c)), in which  $N \times N$  identical SQUIDs are arranged on a tetragonal lattice ( $d_x = d_y$ ), and they are coupled to their nearest-neighbors through magnetic dipole-dipole forces due to their mutual inductance  $M$ . The dynamic equations for the (normalized) flux through the ring of the  $(n, m)$ th SQUID,  $\phi_{n,m}$ , are given by [25, 26]

$$\ddot{\phi}_{n,m} + \gamma \dot{\phi}_{n,m} + \phi_{n,m} + \beta \sin(2\pi\phi_{n,m}) = \phi_{n,m}^{eff}(\tau) + \lambda(\phi_{n-1,m} + \phi_{n+1,m} + \phi_{n,m-1} + \phi_{n,m+1}), \quad (1)$$

where  $n, m = 1, \dots, N$ , and

$$\phi_{n,m}^{eff} = \phi_{n,m}^{ext} - \lambda(\phi_{n-1,m}^{ext} + \phi_{n+1,m}^{ext} + \phi_{n,m-1}^{ext} + \phi_{n,m+1}^{ext}), \quad (2)$$

with

$$\phi_{n,m}^{ext} = \phi_{n,m}^{dc} + \phi_{ac} \cos(\Omega\tau) \quad (3)$$

In Eqs. (1)-(3),  $\lambda = M/L$  is the coupling strength between neighboring SQUIDs, and

$$\beta = \frac{\beta_L}{2\pi} = \frac{L I_c}{\Phi_0}, \quad \gamma = \omega_{LC} \frac{L}{R}, \quad (4)$$

is the rescaled SQUID parameter and loss coefficient, respectively, with  $\omega_{LC} = 1/\sqrt{LC}$  being the inductive-capacitive ( $LC$ ) or geometrical SQUID frequency ( $\Phi_0$  is the flux quantum). The overdots on  $\phi_{n,m}$  denote differentiation with respect to the temporal variable  $\tau$  (normalized to  $\omega_{LC}^{-1}$ ). For applying a dc flux gradient along the direction of increasing  $n$ , a dc flux function of the form

$$\phi_{n,m}^{dc} = \frac{n-1}{N-1} \phi_{dc}^{max}, \quad (5)$$

where  $n, m = 1, \dots, N$  is assumed. Thus, the dc flux increases linearly from zero (for the SQUIDs at  $(n, m) = (1, m)$ ,  $m = 1, \dots, N$ ) to  $\phi_{dc}^{max}$  (for the SQUIDs at  $(n, m) = (N, m)$ ,  $m = 1, \dots, N$ ). For the numerical simulations, the experimentally relevant model parameters  $\beta_L = 0.86$ ,  $\gamma = 0.01$ , and  $\lambda = -0.02$ , have been adopted [27]. The driving frequency has been chosen to be close to the geometrical resonance, i.e.,  $\Omega = 1.01$ , where individual SQUIDs exhibit extreme multistability [24].

### III. GENERATION AND CONTROL OF CHIMERA STATES.

Eqs. (1) are integrated numerically in time using a standard fourth-order Runge-Kutta algorithm with time-step  $h = 0.02$  and free-end boundary conditions. For any parameter set, Eqs. (1) are initialized with zeros, i.e., with

$$\phi_{n,m}(\tau = 0) = 0, \quad \dot{\phi}_{n,m}(\tau = 0) = 0, \quad \text{for any } n, m. \quad (6)$$

Time-integration for  $10^4 T$  time-units, where  $T = 2\pi/\Omega$  is the driving period, is allowed for transients to die-out

and a ‘‘steady-state’’ to be reached. In Figs. 2 and 3, the averages of  $\dot{\phi}_{n,m}(\tau)$  over a driving period  $T$ , i.e.,

$$\langle \dot{\phi}_{n,m} \rangle_T = \frac{1}{T} \int_0^T \dot{\phi}_{n,m} d\tau, \quad (7)$$

are mapped on the  $n - m$  plane for  $\phi_{ac} = 0.02$  and  $\phi_{ac} = 0.04$ , respectively, and several values of  $\phi_{dc}^{max}$  (which determines the value of the gradient of the dc flux). In these maps, areas of uniform (resp. nonuniform) colorization indicate that the SQUID oscillators there are synchronized (resp. desynchronized).

For low  $\phi_{dc}^{max}$ , the SQUID metasurface is in an almost spatially homogeneous state. With increasing  $\phi_{dc}^{max}$  (or equivalently by increasing flux gradient), a threshold is reached at which some of the SQUIDs close to the  $n = N$  end become desynchronized with respect to the others, and the spatially homogeneous state breaks down. In Fig. 2, the breaking of the spatially homogeneous state of the SQUID metasurface occurs at  $\phi_{dc}^{max} = 0.27$  (Fig. 2(a)). With further increase of  $\phi_{dc}^{max}$ , more and more SQUIDs close to  $n = N$  become desynchronized (Fig. 2(b)) until they form a well-defined desynchronized (incoherent) cluster at  $\phi_{dc}^{max} = 0.33$  (Fig. 2(c)). That incoherent cluster begins to shift towards the  $n = 1$  end with  $\phi_{dc}^{max}$  increasing yet further (Fig. 2(d) - 2(g)), i.e., from  $\phi_{dc}^{max} = 0.33$  to  $\phi_{dc}^{max} = 0.45$ . For values of  $\phi_{dc}^{max}$  in this interval, the width of the incoherent cluster remains approximately the same. In Figs. 2(h) - 2(l), i.e., from  $\phi_{dc}^{max} = 0.48$  to  $\phi_{dc}^{max} = 0.60$ , the incoherent cluster continues to shift towards the  $n = 1$  end but its width has become narrower. In Fig. 2(i) ( $\phi_{dc}^{max} = 0.51$ ), a second incoherent cluster emerges at  $n \sim N$  which also changes with further increasing  $\phi_{dc}^{max}$ . This effect becomes more clear in Fig. 3, whose parameters differ from those of Fig. 2 only in the value of  $\phi_{ac}$ . In Fig. 3, the threshold value of  $\phi_{dc}^{max}$  for desynchronization to appear at the  $n = N$  end is lower. Indeed, as can be observed clearly in Fig. 3(a), for  $\phi_{dc}^{max} = 0.27$ , the desynchronized cluster is already formed close to the  $n = N$  end (compare with the corresponding Fig. 2(a)). Similarly to what is observed in Fig. 2, the desynchronized cluster shifts with increasing  $\phi_{dc}^{max}$  towards the  $n = 1$  end. Its width remains approximately the same from  $\phi_{dc}^{max} = 0.30$  to  $\phi_{dc}^{max} = 0.48$  (Fig. 3(b) - 3(h)). From  $\phi_{dc}^{max} = 0.51$  to  $\phi_{dc}^{max} = 0.60$  (Fig. 3(i) - 3(l)) the desynchronized cluster continues its shifting towards the  $n = 1$  end, while its width becomes somewhat narrower. Here, the formation and shifting of a second desynchronized cluster can be clearly observed (due to higher ac flux amplitude  $\phi_{ac} = 0.04$ ). The second desynchronized cluster appears at the  $n = N$  end in Fig. 3(h) ( $\phi_{dc}^{max} = 0.60$ ), then grows in width and follows the shifting pattern of the first desynchronized cluster. Its width remains approximately the same for  $\phi_{dc}^{max} = 0.54 - 0.60$  (Figs. 3(j) - 3(l)). The emergence of more desynchronized clusters can be observed in larger SQUID metasurfaces, i.e., with larger  $N$ , for sufficiently high values of  $\phi_{dc}^{max}$  (not shown).

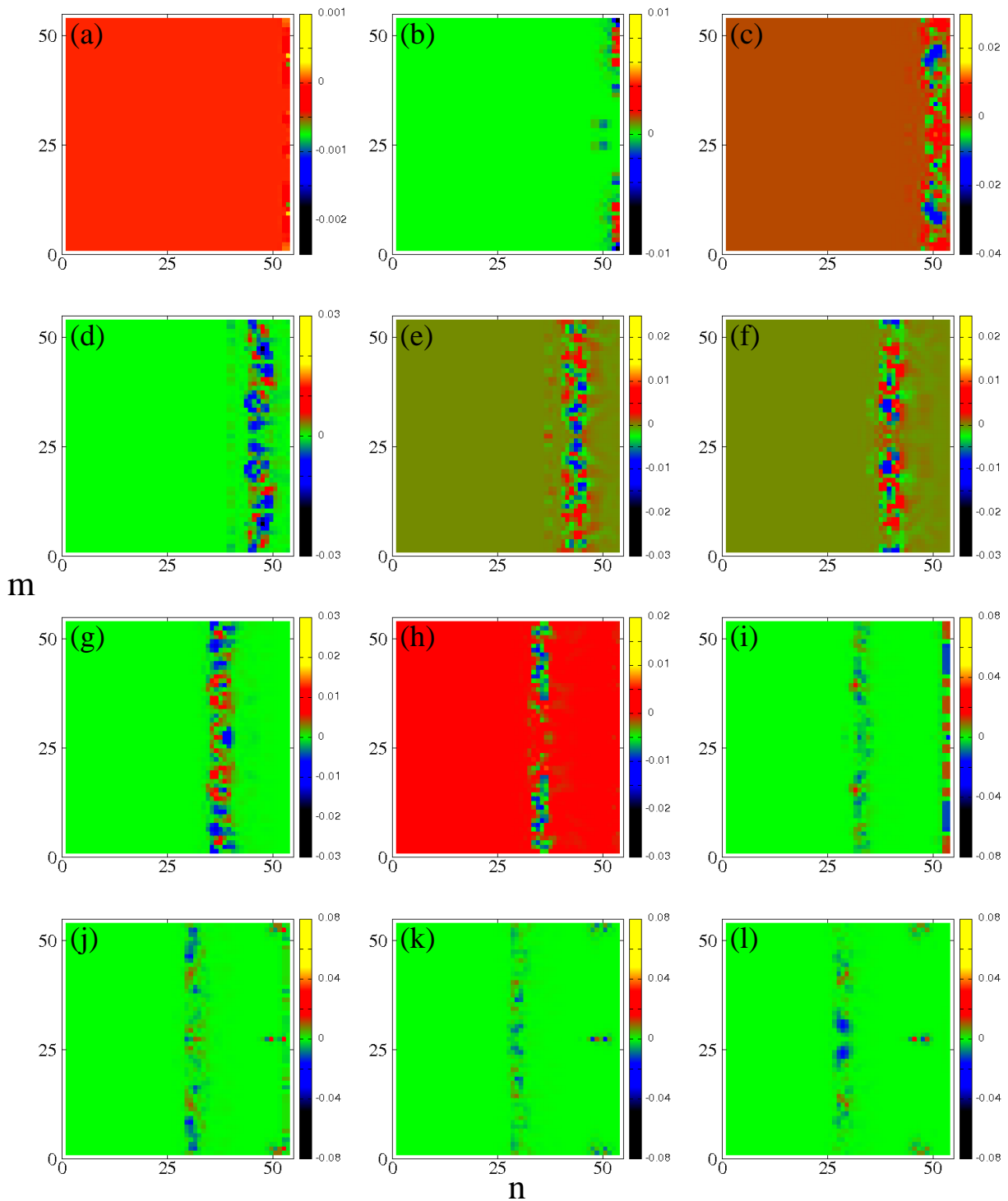


FIG. 2: (Color online) Maps of  $\langle \dot{\phi}_{n,m} \rangle_T$  on the  $n-m$  plane for  $N = 54$ ,  $\beta_L = 0.86$ ,  $\gamma = 0.01$ ,  $\lambda = -0.02$ ,  $\Omega = 1.01$ ,  $\phi_{ac} = 0.02$ , and  $\phi_{dc}^{max}$  from (a) to (l) increases from 0.27 to 0.60 in steps of 0.03.

#### IV. CHARACTERIZATION OF SPATIALLY INHOMOGENEOUS STATES.

Eqs. (1) are integrated in time as above for many values of  $\phi_{ac}$  and  $\phi_{dc}^{max}$  on the  $\phi_{ac} - \phi_{dc}^{max}$  plane. Here, after

the transients have died out, Eqs. (1) are integrated for  $\tau_{sst} = 10^4$  more time-units, while the SQUID metamaterial is in a steady state. The kind of state that has emerged for each pair of  $\phi_{ac}$  and  $\phi_{dc}^{max}$  values can be in-

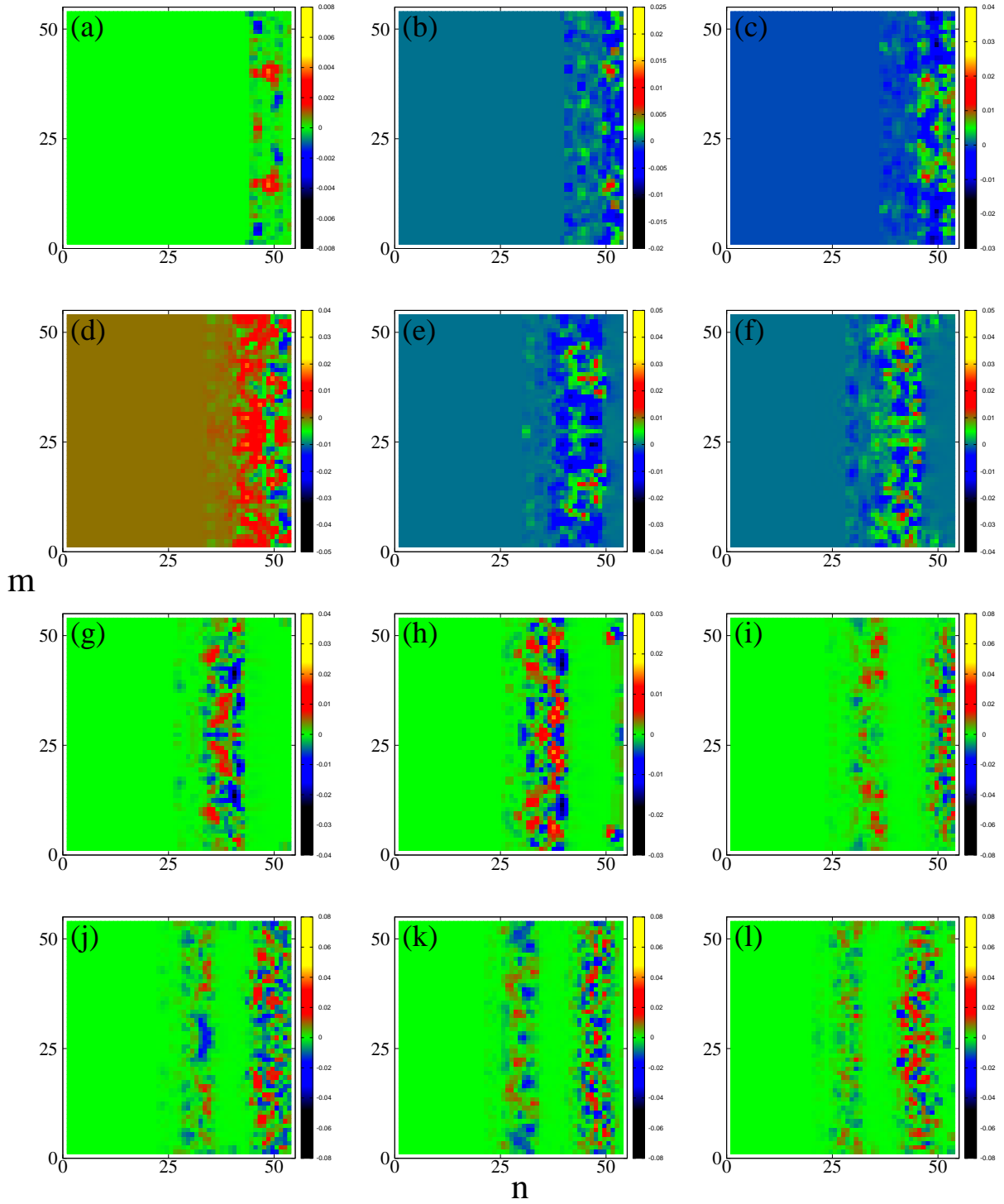


FIG. 3: (Color online) Maps of  $\langle \dot{\phi}_{n,m} \rangle_T$  on the  $n - m$  plane for  $\phi_{ac} = 0.04$  and the other parameters as in Fig. 2.

ferred by calculating several measures which are mapped on the  $\phi_{ac} - \phi_{dc}^{max}$  plane. A global measure of synchronization of the SQUID metasurface is given by

$$\langle r \rangle_{sst} = \frac{1}{\tau_{sst}} \int_0^{\tau_{sst}} r(\tau) d\tau, \quad (8)$$

i.e., by the average over the steady-state integration time  $\tau_{sst}$  of the magnitude of the Kuramoto synchronization

parameter  $r(\tau) = |\Psi(\tau)|$ , where

$$\Psi(\tau) = \frac{1}{N^2} \sum_{n,m} e^{2\pi i \phi_{n,m}(\tau)}. \quad (9)$$

Also, a measure of incoherence and a chimera index for the resulting state can be calculated as follows [28, 29]. First, define

$$u_n(\tau) = \left\langle \frac{1}{N} \sum_{m=1}^N \dot{\phi}_{n,m} \right\rangle_T(\tau) \quad (10)$$

where the angular brackets indicate averaging over the driving period  $T$ , and its local spatial average in a region of length  $n_0 + 1$  around the site  $n$  at time  $\tau$ ,

$$\bar{u}_n(\tau) = \frac{1}{n_0 + 1} \sum_{n=-n_0/2}^{+n_0/2} u_n(\tau), \quad (11)$$

where  $n_0 < N$  is an integer. Then, the local standard deviation of  $u_n(\tau)$  is defined as

$$\sigma_n(\tau) \equiv \left\langle \sqrt{\frac{1}{n_0 + 1} \sum_{n=-n_0/2}^{+n_0/2} (u_n - \bar{u}_n)^2} \right\rangle_{sst}, \quad (12)$$

where the large angular brackets denote averaging over  $\tau_{sst}$ . The index of incoherence and the chimera index is then defined as

$$S = 1 - \frac{1}{N} \sum_{n=1}^N s_n, \quad \eta = \frac{1}{2} \sum_{n=1}^N |s_n - s_{n+1}|, \quad (13)$$

respectively, where  $s_n = \Theta(\delta - \sigma_n)$  with  $\Theta$  being the Theta function. The index  $S$  takes its values in  $[0, 1]$ , with 0 and 1 corresponding to synchronized and desynchronized states, respectively, while all other values between them indicate a chimera or multi-chimera state. The index  $\eta$  equals to unity (an integer greater than unity) for a chimera (a multi-chimera) state. It roughly provides the number of desynchronized clusters or ‘‘heads’’ of the (multi-)chimera state.

In Fig. 4, the measures  $\langle r \rangle_{sst}$ ,  $S$ , and  $\eta$ , calculated from Eqs. (8) and (13), are mapped on the  $\phi_{dc}^{max} - \phi_{ac}$  plane. In Fig. 4(a), for values of  $\phi_{dc}^{max}$  and  $\phi_{ac}$  within the green area, in which  $\langle r \rangle_{sst} \simeq 1$ , the SQUID metamaterial is in a state with a high degree of synchronization (almost synchronized state). In the rest of the plane,  $\langle r \rangle_{sst}$  takes values significantly less than unity, indicating that the SQUID metamaterial is in a partially synchronized or in a completely desynchronized state. However, it cannot be concluded from  $\langle r \rangle_{sst}$  alone whether a particular state is partially or completely desynchronized, and furthermore it cannot be concluded whether a partially synchronized state is a chimera or multi-chimera state or another type of spatially inhomogeneous state. For that purpose, the information in Figs. 4(b) and (c)

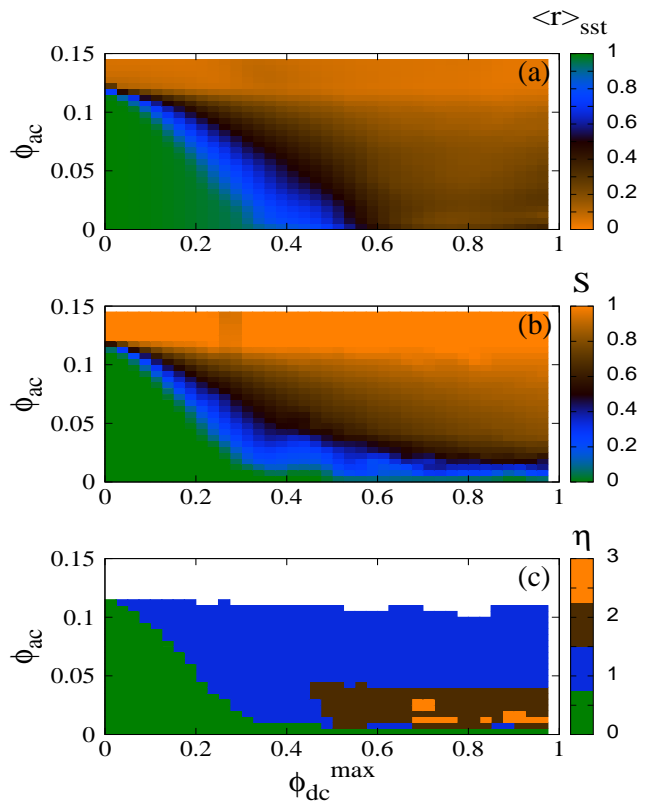


FIG. 4: (Color online) Maps of (a) the magnitude of the synchronization parameter averaged over the steady-state integration time  $\tau_{sst}$ ,  $\langle r \rangle_{sst}$ , (b) the incoherence index  $S$ , and (c) the chimera index  $\eta$ , on the  $\phi_{dc}^{max} - \phi_{ac}$  plane for  $N = 54$ ,  $\beta_L = 0.86$ ,  $\gamma = 0.01$ ,  $\lambda = -0.02$ , and  $\Omega \simeq 1.01$ .

for the the incoherence index  $S$  and the chimera index  $\eta$  has to be used. In Fig. 4(b), the incoherence index  $S$  is exactly zero in the green area ( $S = 0$ ), indicating synchronization. It should be noted however that the green areas in Figs. 4(a) and (b) do not completely coincide. Indeed, in Fig. 4(b), the green area extends to  $\phi_{dc}^{max}$  values up to 0.5 (for very low  $\phi_{ac}$ ), for which Fig. 4(a) gives  $\langle r \rangle_{sst}$  significantly less than unity. This apparent contradiction is discussed in the next paragraph. The chimera index  $\eta$ , mapped in Fig. 4(c), provides information for the number of ‘‘heads’’ of a chimera/multi-chimera state, i.e., the number of desynchronized clusters. In the green area, that number is zero as it should be, while it is one, two, and three in the blue, brown, and orange areas, indicating the generation of single-headed, two-headed, and three-headed chimera states, respectively. Note also the white area in Fig. 4(c), for  $\phi_{ac} \gtrsim 0.11$ , for which the incoherence index  $S$  in Fig. 4(b) is exactly unity. In this area, the resulting state of the SQUID metamaterial is completely desynchronized.

As mentioned in the previous paragraph, there is a green narrow strip in Figs. 4(b) and (c) from  $\phi_{dc}^{max} \simeq 0.32$  to 0.98 and very low values of  $\phi_{ac}$ , in which  $S = 0$  and  $\eta = 0$  that indicate a non-chimeric state. At the same

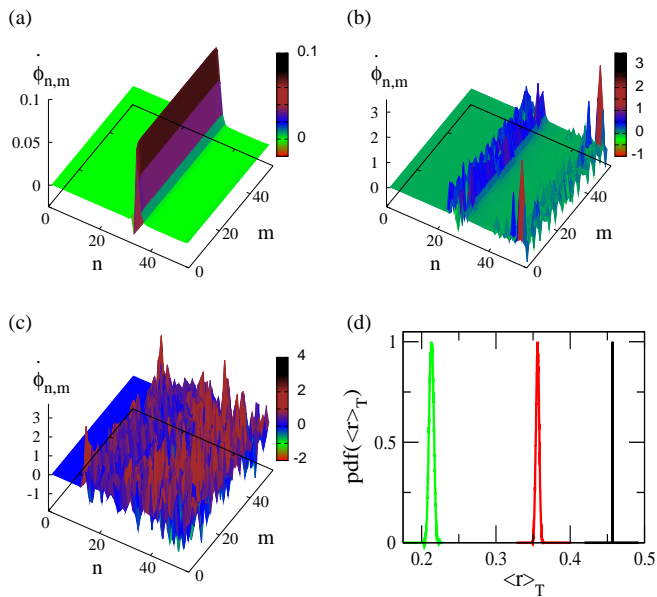


FIG. 5: (Color online) Two-dimensional profiles of  $\dot{\phi}_{n,m}$  for  $\phi_{dc}^{max} = 0.6$ ,  $\beta_L = 0.86$ ,  $\gamma = 0.01$ ,  $\lambda = -0.02$ ,  $\Omega \simeq 1.010N = 54$ , and (a)  $\phi_{ac} = 0.001$ , (b)  $\phi_{ac} = 0.03$ , (c)  $\phi_{ac} = 0.08$ . (d) Probability density functions  $pdf(\langle r \rangle_T)$  for the states in (a), (b), and (c), shown as black, red, and green curves, respectively.

time, the measure  $\langle r \rangle_{sst}$  in the same area assumes values significantly lower than unity ( $\langle r \rangle_{sst} \simeq 0.46$ ), indicating at least partial desynchronization. For clarifying this apparent discrepancy, three spatial profiles are presented in Fig. 5(a), (b), and (c), which are obtained for  $\phi_{dc}^{max} = 0.6$  and  $\phi_{ac} = 0.001$ ,  $0.03$ , and  $0.08$ , respectively. The corresponding pairs of values are located in the green strip, the blue area and the brown area, respectively, of Fig. 4(b). The profile in Fig. 5(a), for  $\phi_{ac} = 0.001$ , is clearly not a chimera state; however, it is not a synchronized state either, since the fluxes in at least two or three SQUIDs oscillate with a high amplitude compared to the fluxes in the rest of them (and also their phases with respect to the driver are generally different). This justifies the low value of  $\langle r \rangle_{sst}$  in Fig. 4(a) (at least partial desynchronization), as well as the value  $S = 0$  (no chimera state) and  $\eta = 0$  (no desynchronized cluster). In Fig. 5(b), for  $\phi_{ac} = 0.03$ , a two-headed chimera state is observed, for which  $\langle r \rangle_{sst} \simeq 0.36$ ,  $S = 0.48$ , and  $\eta = 2$ . In Fig. 5(c), a single-headed chimera state with  $\langle r \rangle_{sst} \simeq 0.21$ ,  $S = 0.81$ , and  $\eta = 1$  is obtained. Thus, although the measures  $S$  and  $\eta$  correctly predict the existence of a chimera state and its “heads”, they cannot discriminate between a synchronized state and a clustered state in which the oscillators in each cluster are synchronized, but the clusters are not synchronized to each other. On the other hand, in such a clustered state,  $\langle r \rangle_{sst} < 1$  indicating at least partial desynchronization. In order to distinguish between such clustered states and synchronized states without inspecting the profiles, additional information is necessary,

which can be provided, e.g., by the probability distribution function of the  $\langle r \rangle_T$  values,  $pdf(\langle r \rangle_T)$ , where

$$\langle r \rangle_T = \frac{1}{T} \int_0^T r(\tau) d\tau. \quad (14)$$

The distributions for the three profiles in Figs. 5(a)-(c) are shown in Fig. 5(d). The full-width half-maximum (FWHM) of the distributions is a measure of metastability for chimera states [30, 31]. However, for states such as that shown in Fig. 5(a), for which  $\langle r \rangle_T$  does not fluctuate in time, the  $pdf(\langle r \rangle_T)$  is practically zero (black curve). For the two chimera states in Figs. 5(b) and (c), the corresponding FWHM is  $\sim 0.005$  and  $\sim 0.007$ , respectively. It should be noted that there are also other measures that could be employed such as, e.g., a measure based on the local curvature of a given state [32]. This measure has been proved particularly useful whenever turbulent chimeras appear, e.g., in semiconductor laser arrays [33, 34].

## V. CONCLUDING.

In the present work it is demonstrated that chimera states can be generated and controlled by a dc flux gradient. Note that the application of a dc flux gradient on a SQUID metamaterial is experimentally feasible with existing experimental set-ups [17]. It is important that by using a dc flux gradient, there is no need for any specific initialization of the SQUID metamaterial to obtain chimera states. The appearance (i.e., the location and size of the desynchronized cluster(s), the number of “heads” of the chimera state) and the degree of synchronization of the chimera states can be controlled to some extent by varying the externally controlled parameters such as the dc flux gradient (determined by  $\phi_{dc}^{max}$ ), and the ac flux amplitude  $\phi_{ac}$ .

Three measures, i.e.,  $\langle r \rangle_{sst}$ ,  $S$ , and  $\eta$ , are calculated and mapped on the  $\phi_{dc}^{max} - \phi_{ac}$  plane. By combining information from all these three measures, the generation or not of a chimera state, and the number of its heads can be anticipated. However, neither of these measures can distinguish between a chimera state and a clustered state in which the SQUIDs within each clusters are synchronized but the clusters are not synchronized to each other. This can be however achieved by calculating an additional quantity, the FWHM of the probability density  $pdf(\langle r \rangle_T)$ ; chimera states are then indicated by nonzero FWHM.

## ACKNOWLEDGMENT

The authors gratefully acknowledge the financial support of the Ministry of Science and Higher Education of the Russian Federation in the framework of Increase Competitiveness Program of NUST “MISiS” (No. K2-2017-006), implemented by a governmental decree dated

16th of March 2013, N 211. This research has been financially supported by General Secretariat for Research

and Technology (GSRT) and the Hellenic Foundation for Research and Innovation (HFRI) (Grant No. 203).

- 
- [1] S. M. Anlage. The physics and applications of superconducting metamaterials. *J. Opt.*, 13:024001–10, 2011.
- [2] P. Jung, A. V. Ustinov, and S. M. Anlage. Progress in superconducting metamaterials. *Supercond. Sci. Technol.*, 27:073001 (13pp), 2014.
- [3] N. Lazarides and G. P. Tsironis. Superconducting metamaterials. *Phys. Rep.*, 752:1–67, 2018.
- [4] N. Lazarides, G. Neofotistos, and G. P. Tsironis. Chimeras in SQUID metamaterials. *Phys. Rev. B*, 91(05):054303 [8 pages], 2015.
- [5] J. Hizanidis, N. Lazarides, and G. P. Tsironis. Robust chimera states in SQUID metamaterials with local interactions. *Phys. Rev. E*, 94:032219, 2016.
- [6] J. Hizanidis, N. Lazarides, G. Neofotistos, and G. P. Tsironis. Chimera states and synchronization in magnetically driven SQUID metamaterials. *Eur. Phys. J.-Spec. Top.*, 225:1231–1243, 2016.
- [7] J. Hizanidis, N. Lazarides, and G. P. Tsironis. Chimera states in networks of locally and non-locally coupled SQUIDs. *Frontiers in Applied Mathematics and Statistics*, submitted (2018).
- [8] Y. Kuramoto and D. Battogtokh. Coexistence of coherence and incoherence in nonlocally coupled phase oscillators. *Nonlinear Phenom. Complex Syst.*, 5(4):380–385, 2002.
- [9] M. J. Panaggio and D. M. Abrams. Chimera states: Coexistence of coherence and incoherence in network of coupled oscillators. *Nonlinearity*, 28(3):R67–R87, 2015.
- [10] E. Schöll. Synchronization patterns and chimera states in complex networks: Interplay of topology and dynamics. *Eur. Phys. J.-Spec. Top.*, 225:891–919, 2016.
- [11] Nan Yao and Zhigang Zheng. Chimera states in spatiotemporal systems: Theory and applications. *Int. J. Mod. Phys. B*, 30:1630002 (44 pages), 2016.
- [12] T. Isele, J. Hizanidis, A. Provata, and P. Hövel. Controlling chimera states: The influence of excitable units. *Phys. Rev. E*, 93:022217, 2016.
- [13] J. Sieber, O. E. Omelchenko, and M. Wolfrum. Controlling unstable chaos: Stabilizing chimera states by feedback. *Phys. Rev. Lett.*, 112:054102, 2014.
- [14] V. Semenov, A. Zakharova, Y. Maistrenko, and E. Schöll. Delayed-feedback chimera states: Forced multiclusters and stochastic resonance. *Europhys. Lett.*, 115:10005, 2016.
- [15] L. V. Gambuzza and M. Frasca. Pinning control of chimera states. *Phys. Rev. E*, 94:022306, 2016.
- [16] C. Bick and E. A. Martens. Controlling chimeras. *New J. Phys.*, 17:033030, 2015.
- [17] Daimeng Zhang, M. Trepanier, O. Mukhanov, and S. M. Anlage. Broadband transparency of macroscopic quantum superconducting metamaterials. *Phys. Rev. X*, 5:041045 [10 pages], 2015.
- [18] A. P. Zhuravel, A. V. Ustinov, M. Trepanier, Daimeng Zhang, and S. M. Anlage. Imaging microwave response of rf-SQUID metasurface in dc magnetic field. *9th International Kharkiv Symposium on Physics and Engineering of Microwaves, Millimeter and Submillimeter Waves (MSMW)*, DOI:10.1109/MSMW.2016.7538200, 2016.
- [19] A. S. Averkin, A. P. Zhuravel, P. Jung, N. Maleeva, V. P. Koshelets, L. V. Filippenko, A. Karpov, and A. V. Ustinov. Imaging coherent response of superconducting metasurface. *IEEE Trans. Appl. Supercond.*, 26(3):1–3, 2016.
- [20] A. Karpov, A. P. Zhuravel, A. S. Averkin, V. I. Chichkov, and A. V. Ustinov. Phase-sensitive imaging of microwave currents in superconductive circuits. *arXiv*; arXiv:1804.03026, 2018.
- [21] B. Josephson. Possible new effects in superconductive tunnelling. *Phys. Lett. A*, 1:251–255, 1962.
- [22] J. Clarke and A. I. Braginski. *The SQUID Handbook Vol. I: Fundamentals and Technology of SQUIDs and SQUID Systems*. Wiley-VCH, Weinheim, Germany, 2004.
- [23] J. Clarke and A. I. Braginski. *The SQUID Handbook Vol. II: Applications of SQUIDs and SQUID Systems*. Wiley-VCH, Weinheim, Germany, 2004.
- [24] J. Hizanidis, N. Lazarides, and G. P. Tsironis. Flux bias-controlled chaos and extreme multistability in SQUID oscillators. *Chaos*, 28:063117 [8 pages], 2018.
- [25] N. Lazarides and G. P. Tsironis. Multistability and self-organization in disordered SQUID metamaterials. *Supercond. Sci. Technol.*, 26:084006 (12pp), 2013.
- [26] G. P. Tsironis, N. Lazarides, and I. Margaritis. Wide-band tuneability, nonlinear transmission, and dynamic multistability in SQUID metamaterials. *Appl. Phys. A*, 117:579–588, 2014.
- [27] M. Trepanier, Daimeng Zhang, O. Mukhanov, and S. M. Anlage. Realization and modeling of rf superconducting quantum interference device metamaterials. *Phys. Rev. X*, 3:041029, 2013.
- [28] R. Gopal, V. K. Chandrasekar, A. Venkatesan, and M. Lakshmanan. Observation and characterization of chimera states in coupled dynamical systems with non-local coupling. *Phys. Rev. E*, 89:052914, 2014.
- [29] R. Gopal, V. K. Chandrasekar, D. V. Senthilkumar, A. Venkatesan, and M. Lakshmanan. Chimera at the phase-flip transition of an ensemble of identical nonlinear oscillators. *Commun. Nonlinear Sci. Numer. Simulat.*, 59:30–46, 2018.
- [30] M. Shanahan. Metastable chimera states in community-structured oscillator networks. *Chaos*, 20:013108, 2010.
- [31] M. Wildie and M. Shanahan. Metastability and chimera states in modular delay and pulse-coupled oscillator networks. *Chaos*, 22:043131, 2012.
- [32] F. P. Kemeth, S. W. Haugland, L. Schmidt, I. G. Kevrekidis, and K. Krischer. A classification scheme for chimera states. *Chaos*, 26:094815, 2016.
- [33] J. Shena, J. Hizanidis, P. Hövel, and G. P. Tsironis. Multiclustered chimeras in large semiconductor laser arrays with nonlocal interactions. *Phys. Rev. E*, 96:032215, 2017.
- [34] J. Shena, J. Hizanidis, V. Kovanis, and G. P. Tsironis. Turbulent chimeras in large semiconductor laser arrays. *Sci. Rep.*, 7:42116, 2017.